Using growth and geochemical composition of Clathromorphum compactum to track multiscale North Atlantic hydro-climate variability

Valentin Siebert, Pierre Poitevin, Laurent Chauvaud, Bernd R. Schöne, Pascal Lazure, Julien Thébault

Using growth and geochemical composition of *Clathromorphum compactum* to track multiscale North Atlantic hydro-climate variability

Valentin Siebert*[1], Pierre Poitevin[1-4], Laurent Chauvaud[1], Bernd R. Schöne[2], Pascal Lazure[3], Julien Thébault[1]

[1] *Université de Bretagne Occidentale, Laboratoire des Sciences de l'Environnement Marin (UMR6539 UBO/CNRS/IRD/Ifremer), 29280 Plouzané, France*

[2] *Institute of Geosciences, University of Mainz, Johann-Joachim-Becher-Weg 21, 55128 Mainz, Germany*

[3] *Ifremer, Laboratoire d'Océanographie Physique et Spatiale (UMR6523 CNRS/Ifremer/IRD/UBO), 29280 Plouzané, France*

Email addresses:

Valentin Siebert (corresponding author): valentin.siebert@univ-brest.fr

Pierre Poitevin: pierre.poitevin@univ-brest.fr

Julien Thébault: julien.thebault@univ-brest.fr

Bernd R. Schöne: schoeneb@uni-mainz.de

Pascal Lazure: pascal.lazure@ifremer.fr

Laurent Chauvaud: laurent.chauvaud@univ-brest.fr

[4] present address: Fisheries and Oceans Canada, Maurice Lamontagne Institute, Mont-Joli, QC, Canada

Highlights

- A new method for growth measurements based on Mutvei's solution staining

- High intra- and inter-specimen reproducibility of Mg/Ca and Ba/Ca distribution

- Growth of *C. compactum* is significantly correlated with major hydro-climatic drivers

- Mg/Ca distribution within algae calcite matrix correlates with SST around SPM

- Ba/Ca is significantly correlated with Labrador Current transport

Abstract

Records of ocean/atmosphere dynamics over the past centuries are essential to understand processes driving climate variability. This is particularly true for the Northwest Atlantic which is a key region with an essential role in global climate regulation. Over the past two decades, coralline red algae have been increasingly used as environmental and climatic archives for the marine realm and hold the potential to extend long-term instrumental measurements. Here, we investigate the possibility to extract climate and environmental information from annual growth patterns and geochemical composition of the coralline red algae, *Clathromorphum compactum*, from Saint-Pierre & Miquelon (SPM), a French archipelago southwest of Newfoundland. However, measurements of *C. compactum* growth trends is challenging due to difficulties in identifying annual growth lines directly. So far, growth pattern investigations were commonly performed based on geochemical data of coralline calcite matrix. Nonetheless, this method is expensive and therefore prevents from analysing a large number of specimens that would be representative of the population. For this reason, we enhanced the growth line readability by staining polished sections with Mutvei's solution and performed growth analysis based on direct increment width measurements. Geochemical analyses were also carried out in order to validate the assumption that growth lines observed after staining were formed on an annual basis. Moreover, growth pattern and trace element composition were measured on multiple axes of several individuals in order to assess the intra- and inter-specimen variability and validate their use for paleoenvironmental reconstructions. Finally, relationships between the *C. compactum* sclerochronological records from SPM and environmental datasets covering different geographical areas allow a better knowledge of flow dynamics in the Northwest Atlantic and confirm the findings related to *Arctica islandica* from the same location.

Keywords: sclerochronology; coralline algae; environmental proxy; climate change; environmental reconstruction

1. Introduction

The Northwest Atlantic Ocean is a key region with respect to climate variability as it represents the starting point of the Atlantic Meridional Overturning Circulation (AMOC) which is an important and active component of the climate system (e.g. Rahmstorf, 2003). Southern Newfoundland's coast and the Saint-Pierre & Miquelon (SPM) region lie at the confluence of the main oceanographic currents ruling the North Atlantic Basin (Poitevin et al., 2019) (Figure 1). However, despite its importance, the physical flow dynamics of this region is poorly understood (Wu et al., 2012). This gap mainly exists because of the lack of long-term environmental records in this area before the mid-20th century (Halfar et al., 2011).

Proxy data allow us to generate such records retrospectively and are of crucial importance to extend our knowledge of past environmental conditions. In the oceanic realm, carbonate hard structures of long-lived marine species hold the potential to generate such proxy data to extend instrumental observations by several decades to centuries. While multi-centennial reconstructions of tropical marine hydro-climates have been generated since the 1990's using corals (e.g. Dunbar et al., 1994; Saenger et al., 2009), long term records of environmental conditions in higher latitude oceans are scarce and sparse. In the Northwest Atlantic Ocean, geochemical and growth analyses of the bivalve *Arctica islandica* supply the bulk of annual to subannual resolution extra-tropical marine climate data for near-surface water masses (see Schöne (2013) for a review). While growth increment widths of long-lived bivalves have resulted in numerous climate reconstructions (e.g., Wanamaker et al., 2008; Butler et al., 2013), they also have limitations related to ontogenetic growth trends (Goodwin et al., 2009) and/or biogeographical distribution (Dahlgren et al., 2000).

In an attempt to overcome some of these issues, a few studies focused on the use of coralline red algae as archives of environmental and climatic variability in oceans (e.g., Kamenos et al., 2008; Williams et al., 2011, Halfar et al., 2011). In the Northwest Atlantic Ocean, the species

Clathromorphum compactum (Kjellman 1898) (Rhodophyta; Hapalidiaceae) forms clear annual growth increments which paved the way towards sclerochronological investigations (Moberly, 1968). *C. compactum* specimens show a fairly constant growth rate throughout its lifespan and is not subject to an ontogenetic growth trend (Halfar et al., 2011). Thus, there is no loss of data accuracy in the ontogenetically oldest portions of the specimen. Furthermore, its long lifespan (> 600 years, Halfar et al., 2013) allows very long reconstructions. According to previous studies, growth lines are formed during late winter/early spring (Moberly, 1968) due to a cessation in specimen development between January and April (Halfar et al., 2008; Halfar et al., 2011) resulting in two distinct morphological structures: i) large cells with thinly calcified walls (forming the bulk of the growth increment), and ii) small cells with densely calcified walls (growth line boundary delineating individual increments) (Adey, 1965; Moberly, 1968). Finally, thanks to the wide distribution of *C. compactum* around the Arctic and Sub-Arctic (in North Atlantic and North Pacific Oceans) (Hetzinger et al., 2011; Adey et al., 2013), paleoenvironmental reconstructions are possible at a large spatial scale. Since 1950, past environmental variability has been investigated using the geochemical composition of *Clathromorphum spp.* calcite matrix (e.g. Chave, 1954; Williams et al., 2018). For example, variations in magnesium concentrations of long-lived coralline algae carbonate structure record ambient seawater temperature over time (Moberly, 1968), while barium content provides information about variations in salinity (Hetzinger et al., 2011, Hetzinger et al., 2013) or river runoff (Chan et al., 2011).

In the Northwest Atlantic Ocean, some studies successfully related growth patterns of *C. compactum* to environmental factors such as sea surface temperature (SST) fluctuations (e.g. Chave, 1954; Halfar et al., 2011) or used algal growth trends to develop new proxy (e.g. Halfar et al., 2013; Hetzinger et al., 2019) and extend climatic times-series (e.g. Moore et al., 2017). Nonetheless, extracting increment width measurements from *C. compactum* calcitic matrix is challenging due to the difficulty of identifying annual growth lines with optical or scanning electron

microscopy (Halfar et al., 2011). In addition, the presence of spherical non-calcified reproduction structures, called conceptacles, can also affect growth line readability. The latter have a size that can reach the increment width value and are formed during winter season, when *C. compactum* specimens stop their growth (Moberly, 1968). So far, increment width is mostly measured indirectly through periodic Mg/Ca variations in coralline algae hard strucures (Hetzinger et al., 2011). However, the cost and the time required to collect and process these geochemical data limit our ability to analyse a large number of specimens. This issue raises the questions of sample size and population representativeness, two crucial aspects of sclerochronological studies of growth dynamics.

Currently, some compounds allow the staining of living algae tissues such as alizarin red (Sletten et al., 2017), calcein or calcofluor white (Lewis & Diaz-Pulido, 2017). Nonetheless, these staining methods are applicable in studies on calcification process of living algae, not in long-term paleoenvironmental investigations when periodic growth rates of dead specimens are used as environmental proxies. Since a decade, Mutvei's solution is frequently used to highlight growth structures in many different taxa (bivalve molluscs, gastropods, barnacles, corals, sclerosponges, fish otoliths, cephalopods and whale's tympanic bulla). This solution is composed of glutaraldehyde, acetic acid and alcian blue. Each compound has one specific action on biocarbonates: (i) glutaraldehyde fixates the soluble and insoluble organic matrices, (ii) alcian blue stains mucopolysaccharides, while (iii) acetic acid produces a three-dimensional relief of etch-resistant ridges (growth lines) and etched depressions (growth increments) (Schöne et al., 2005). Although it has been used on several sclerochronological studies so far (e.g. Butler *et al.*, 2013; Poitevin et al., 2019), this technique has never been tested on coralline red algae. However, given Mutvei's solution properties, and *C. compactum* morphological structure, this staining method may be effective to enhance growth lines visibility.

This study focused on growth and geochemical composition of *Clathromorphum compactum* specimens from SPM in order to track multi-scale hydro-climatic dynamics in the Northwest Atlantic region. The objectives of this work are to (i) develop a new method for age determination based on Mutvei's solution staining and direct growth line measurements, and (ii) perform trace element analyses of *C. compactum* hard structures to get a better understanding of hydro-climate variability near SPM and the Northwest Atlantic.

2. Materials & Methods

2.1. Sample preparation

Forty-two specimens of *C. compactum* were collected alive from hard substrates at a depth of 14 m by SCUBA diving along the north coast of Saint-Pierre island (46°49'03”N, 56°09'54”W) the 5th of September 2017 (Figure 1B). The habitat at the sampling site consisted of a rocky shelf.

For each specimen, three cutting axes were defined beforehand perpendicular to the direction of growth (red lines in Figure 2A, B). Specimens were cut along these axes using a precision cutting machine (Struers, Accutom 50; rotation speed 800 rpm, feed rate 100 µm.s-^{1}) equipped with a diamond-coated blade (thickness: 400 µm) continuously cooled by deionized water. The first cutting axis was defined to include the centre of the specimen and thick sections (2mm) were then cut on both sides of this central axis. One was used for the growth measurements (slice 1, in blue, on Figure 2A, B) and the other one for micro-chemical analyses (slice 3, in white, on Figure 2A, B). The two other slices were only used for micro-chemical analyses (slices 2 and 4 on Figure 2A, B) in order to assess intra-specimen variability of trace element distribution. The distance between adjacent cutting axes varied depending on specimen size but never exceeded 6 mm. These sections were mounted on glass microscope slides and carefully ground on a rotating polishing table (Struers, TegraPol-35) with a sequence of 1200 and 2400 grit wet-table carborundum paper, followed by polishing with 3-µm and 1-µm diamond liquid (Struers).

These cross-sections were ultrasonically cleaned with deionized water during few seconds between each grinding or polishing step to remove residual abrasive material. The polished cross-section dedicated to growth measurements (slice 1 on Figure 2A, B) was then etched in a Mutvei's solution (Schöne et al., 2005) for 45 minutes at ambient temperature, soaked in a deionized water bath, and left to air dry before imaging. Treatment with Mutvei's solution results in a three-dimensional display of growth patterns and reveals clear annual growth lines (Figure 2C, D, E and Figure 3B).

2.2. Growth analyses

Stained sections were imaged under reflected light (Zeiss, KL 2500 LCD) using an AxioCam MRc5 RGB camera installed on a Zeiss Lumar.V12 stereomicroscope equipped with a motorized stage (Figure 2C). Photomosaics were constructed using AxioVision 4.9.1 software (Zeiss). The width of the growth increments was measured digitally using the image processing and analysis software ImageJ (NIH Image), from the outer edge of the sample (living portion) to the centre (base of the specimen, attached to the substrate). In order to assess intra-specimen variability, growth rates were measured along several transects (Figure 2C) on slice 1 (Figure 2A, B). The number of transects depended on the global size, morphology and conceptacle position of each sample. As all specimens were live-collected, the last visible increment corresponds to the year of their collection (2017). Thus, a retrospective counting of annual growth increments was sufficient to determine the growth year of each of them (Figure 2D). In order to measure ordinal association between all transects of the same specimen, Spearman's rank correlations of increment width measurements were calculated using R software (R Core Team, 2018). If one transect significantly differed from others (p>0.05), it was removed from the growth analysis dataset. Because of conceptacle density or grazing tracks, accurate counting and measurement of annual increments was performed on seven specimens only.

In order to check whether a common growth signal could be observed between the different *C. compactum* specimens, growth indices (GIs) were calculated for each year by dividing the measured increment width ($L_{t+1} - L_t$) by a predicted increment width ($L(p)_{t+1}$-$L(p)_t$). We assumed that there was no ontogenetic trend in annual growth rate throughout specimen lifespan. Thus, the annual predicted increment width ($L(p)_{t+1}$-$L(p)_t$) should be identical from the base to the top of the specimen. Therefore, this value was defined individually as the arithmetic mean of the increment width values obtained from the different transects.

$$GI_t = \frac{L_{t+1} - L_t}{L(p)_{t+1} - L(p)_t} \quad (1)$$

Individual time-series of GI were then standardized as follows (Schöne, 2013):

$$SGI_t = \frac{GI_t - \mu}{\sigma} \quad (2)$$

Where μ is the average and σ the standard deviation of all GI values. The standardized GI (SGI) is a dimensionless measure of how growth deviates from the predicted trend. Positive values represent greater than expected growth, whereas negative values represent less than expected growth. For the rest of the manuscript, the SGI master-chronology obtained via direct growth lines reading will be noted as SGI_{direct}. The robustness of the SGI_{direct} chronology was tested by calculating the inter-series correlation coefficient. This value corresponds to the average of the correlations between each individual growth series and the mean of all other series. All these analyses were carried out using the R package dplR (Bunn, 2008) and the program COFECHA (Grissino-Mayer, 2001).

2.3. Trace element analyses

Three specimens (CC9; CC25; CC29) with the highest potential to record paleoenvironmental data were selected for trace element analyses based on their vertical height and conceptacles location which allow the longest continious laser path. Three cross-sections (slices 2, 3 and 4 on Figure 2A, B) were cut from each of these specimens and three LA-ICP-MS

transects were analyzed on each of these sections (Figure 3A). These nine transects were parallel to the direction of growth and defined to avoid as much as possible conceptacle cavities and recalcified healed tissue from grazing.

Trace element concentrations were measured with a Thermo Scientific XSERIES 2 quadrupole inductively coupled plasma mass spectrometer (ICP-MS) coupled to a 193 nm laser ablation system (COMPexPro 102, Coherent Inc.) at the Pôle Spectrométrie Océan (European Institute for Marine Studies, Plouzané, France). This setting was used with a laser energy density of 15 $J.cm^{-2}$, a pulse rate of 10 Hz, a spot size of 120 µm and a scan speed of 5 $\mu m.s^{-1}$. Helium was used as carrier gas with a flow rate of 250 $mL.min^{-1}$. Measurements were acquired every 2.28 s, corresponding to an integrated step of around 11.4 µm.

During acquisition, signal intensities (counts per second = cps) were recorded for ^{25}Mg, ^{43}Ca, and ^{137}Ba. Element intensity was systematically normalized against the ^{43}Ca signal (internal standard) to correct for laser beam energy drift, focus variation at the sample surface, and ICP-MS detection drift. The glass reference material NIST SRM 612 was used as a calibration standard with the values of GeoReM database (Jochum et al., 2005). Finally, the detection limits of elements were 9.03 $\mu mol.mol^{-1}$ for magnesium and 0.08 $\mu mol.mol^{-1}$ for barium. Before and after each transect, three external standard runs were performed. Data processing (including instrumental drift correction and normalization) was performed using the R package ElementR (Sirot et al., 2017). Element-to-calcium ratios are expressed in $mmol.mol^{-1}$ (Mg/Ca) and $\mu mol.mol^{-1}$ (Ba/Ca).

Once geochemical analyses were performed, each cross-section was stained with Mutvei's solution to assign calendar dates to geochemical data (Figure 3B). As all samples were collected alive, the top layer was assigned to the year of collection, 2017, and calendar years were assigned to annual growth increments starting from 2017 and extending back in time. This staining step aimed at checking each growth line position in relation to geochemical signals. For this purpose,

we performed growth line readings next to each laser path spread over the three studied specimens (Figure 3B). To allow a better intra- and inter-specimens comparison of geochemical data, the algal Mg/Ca and Ba/Ca time-series were linearly interpolated between these anchor points using the AnalySeries software (Paillard et al., 1996) to generate an equidistant proxy time-series and monthly resolved trace element data. For this purpose, we assume that growth rate was constant during the development period of the algae.

Based on the annual cycles of Mg/Ca time-series measured on the three ablated specimens, we extracted annual increment widths by measuring the distance between two consecutive Mg/Ca minima (e.g. Halfar et al., 2011). The obtained growth data underwent the same statistical treatment as stated above (see section 2.2) and were recovered only from the three geochemical transects performed on slices 3, mirror of slice 1 (Figure 2A, B). Then, we established a SGI master-chronology (noted $SGI_{indirect}$) and we checked its robustness by calculating its inter-series correlation coefficient and by comparing this time-series with the SGI_{direct} chronology previously constructed.

2.4. Comparison with environmental datasets

Poitevin et al. (2019) showed that growth rate of the bivalve *Arctica islandica* from Saint-Pierre and Miquelon is linked to multi-scale hydro-climatic forcing and interactions. Thus, our algal SGI_{direct} master-chronology was compared, via Spearman's rank correlations, with annual climatic indices reflecting climate and ocean dynamics over the North Atlantic Ocean: the Atlantic Meridional Oscillation (AMO) (Knight et al., 2006), the North Atlantic Oscillation (NAO) (Hurrell et al., 2001; Wanner et al., 2001), the Arctic Oscillation (AO) (Thompson & Wallace, 1998) and the Sub-Polar Gyre index (SPG) (Berx & Payne, 2017).

The AMO is represented by an index that reflects SST variations in the low- and mid-latitudes of the north Atlantic basin (0°N – 65°N). Over the time, it oscillates between negative and positive phases that correspond to negative and positive SST anomalies respectively, with a periodicity of ca. 60 years. The dataset used in this study extends from 1966 to 2016.

The NAO index describes the difference of sea-level pressure between the Azores High and Iceland Low. In this region, the negative (positive) phase of the NAO is related to (i) lower (stonger) north-westerly winds, (ii) a reduction (enhancement) in heat losses by the ocean, (iii) a decrease (increase) in deep convection in the Labrador Sea and (iv) a weaker (greater) sea ice coverage over the Newfoundland shelf (Wanner et al., 2001). The AO is an index similar to the NAO, but it is more relevant to the Arctic regions. The NAO and AO databases used in this study cover the time interval from 1950 to 2017.

Finally, the SPG time-series used in this study, covering 1983 to 2015 (Berx & Payne, 2017), are based on maps of sea surface height. Similarly to the other indices, SPG index oscillates between positive and negative phases reflecting different water mass dynamics. Combinations of a strong sub-polar gyre circulation with a wide spread and a strong Labrador current (LC) transport over the Labrador and northeastern Newfoundland Slope appear as positive values. Negative SPG values are associated with a weak sub-polar gyre with a westward retraction and a weak LC.

Furthermore, spatial correlation between algal SGI_{direct} and North Atlantic ocean temperature (averaged from the surface to 100 m water depth, NOAA-NODC) was assessed using KNMI Climate Explorer (https://climexp.knmi.nl/ - last visit in June 2020). Mg/Ca time-series were compared with recorded surface water temperatures from the oceanographic station 27 (47.55°N, 52.583°W) (Figure 1) and to NOAA_ERSST_v4 satellite-based SST values extracted from a 200 km² area around the island of Saint-Pierre. Moreover, we calculated linear regressions between the latter SST database and Mg/Ca distribution. Equation slopes and y-intercepts obtained for these three specimens were compared using a Student t-test in order to test whether magnesium was

included in the same way through the three studied specimens in response to SST variations over the time. Ba/Ca ratios, were compared with recorded surface salinity values from station 27 (Figure 1A) and with the Labrador Current (LC) transport along the Tail of Grand Bank (Figure 1) at several transects from 1992 to 2013 which are available at: http://www.meds-sdmm.dfo-mpo.gc.ca (last visit in June 2020).

3. Results

3.1. Growth analyses

3.1.1. Intra-specimen variability in growth rate

Treatment with Mutvei's solution resulted in a colored three-dimensional display of growth patterns and revealed clear annual growth lines. An alternating pattern of thin dark lines and wide light-colored areas was observed when viewed under reflected light, corresponding respectively to growth lines and increments. This differential staining resulted in etch-resistant ridges of ca. 10 µm height (growth lines) and etched depressions (growth increments), and stained skeletal growth structures in shadings of blue (Figure 2C, D, E).

Number of transects read on slices 1 (Figure 2A, B) for increment width measurements differed between each cross-section, ranging from 2 to 7 transects per specimen (with an averaged number of 4.42 ± 1.72 transects per specimen). Most increment width time-series obtained from these measured transects were significantly positively correlated with each other. Nevertheless, some transects were significantly different: T4 in specimens CC2 and CC7, T2, T6 and T7 in specimen CC13, and T1 in specimen CC29 (Figure 4). These transects were discarded from the dataset.

3.1.2. Population-scale growth signal and chronologies construction

Between 1988 and 2016, the average annual increment width of *C. compactum* was 248 µm ± 69 µm. This value was obtained based on the annual growth increments of the seven studied specimens (Figure 5A). The inter-series correlation coefficient calculated from the seven SGI_{direct}

time-series was 0.33. The SGI_{direct} varied considerably over the entire chronology, ranging from a minimum of -1.3 in 1993 to a maximum of 2.2 in 2003. In general, SGI_{direct} values were mostly negative from 1970 to 1998 and became positive afterwards (Figure 5A). While a lower inter-series correlation coefficient was found for the $SGI_{indirect}$ master-chronology (0.26), the growth variability between 1988 and 2016 is positively and significantly correlated to the SGI_{direct} signal (r = +0.37; $p<0.05$) (Figure 5). Nonetheless, because of this weaker inter-series coefficient correlation and the limited sample depth, we will only compare the growth signals extracted via direct measurements (SGI_{direct}) to the environmental parameters.

3.2 Trace elements

3.2.1 Trace elements distribution

As expected, Mg/Ca variations followed a cyclic annual pattern with maximum values close to the centre of the growth increments and minimum values at or close to the growth lines (Figure 6). Ba/Ca also showed a cyclic annual pattern, a bit more noisy and inversely correlated with Mg/Ca variations (r = -0.31, *p<0.05*). Furthermore, maximum Ba/Ca values usually appeared close to growth lines, while minimum values occurred in the middle of the increments. Nonetheless, extreme Mg/Ca and Ba/Ca values did not always perfectly correspond with growth lines, but were observed a few microns before or after the growth lines (Figure 6). Moreover, geochemical signals are more variable in the oldest parts of the records, especially for CC25 and CC29. This is likely due to the difficulty we had to avoid conceptacles at the basis of cross-sections because of their high density. In addition, only one transect represents the average element-to-calcium ratios which makes the signal more sensitive to outliers.

3.2.2 Intra/inter-specimen trace element distribution

Spearman's rank correlation coefficients were calculated for each specimen and each element in order to compare pairs of transects (Figure 7). In each specimen, Mg/Ca series were all significantly correlated, with only one exception (between transects T3 and T4 for CC29). That was

also the case for Ba/Ca in which 32 out of 36 pairs of series were significantly correlated. Given the high intra-specimen reproducibility, the Mg/Ca and Ba/Ca time-series for each specimen were averaged for these two elements, without removing any transect.

CC25 specimen had higher average Mg/Ca values than the two others (CC25: Mg/Ca = 200 mmol/mol; CC9 and CC29: Mg/Ca = 135 and 139 mmol/mol respectively) and also lower Ba/Ca average values (CC25: Ba/Ca = 5.80 µmol/mol; CC9 and CC29: Ba/Ca = 19.10 and 19.57 µmol/mol respectively) (Figure 6). Despite this offset, highly significant Spearman's correlations were found between averaged Mg/Ca time-series of CC9 and CC25 (r = +0.78; *p<0.001*), CC29 and CC25 (r = +0.79; *p<0.001*), and CC9 and CC29 (r = +0.77; *p <0.001*). Regarding barium, highly significant Spearman's correlations were also observed between averaged Ba/Ca time-series of the three specimens (r = +0.67; *p<0.001* between CC9 and CC25, r = +0.69; *p<0.001* between CC25 and CC29, r = +0.65; *p<0.001* between CC9 and CC29).

3.3 Link between growth, element chemistry and environmental variables

The SGI_{direct} time-series was compared to NOAA-NODC 0-100m ocean mean temperature (3-month averages) using KNMI climate explorer. In each season, a significant positive correlation was observed between *C. compactum* growth dynamics and SST in the North Atlantic basin, specifically within the subpolar gyre extent (Figure 8). Moreover, the *C. compactum* SGI_{direct} master-chronology was significantly correlated with the annual SPG index between 1993 and 2015 (r = -0.56; $p<0.05$) and with the AMO index between 1996 and 2016 (r = +0.51, $p<0.05$). On the other hand, no significant correlation was found between *C. compactum* SGI_{direct} and the two other atmospheric indices, respectively AO (r = -0.21; $p = 0.13$) and NAO (r = -0.13; $p = 0.36$) for the time intervals from 1966 to 2016.

Furthermore, Mg/Ca variations within coralline red algae carbonate structures are coupled with local satellite-based SST variations. A significant linear relationship exists between monthly

Mg/Ca values of the three studied specimens and monthly data of SST (r^2 = 0.61 and *p<0.05* for CC9, r^2 = 0.45 and *p<0.05* for CC25, r^2 = 0.54 and *p<0.05* for CC29). One calibration equation was then generated for each individual, and their slopes and y-intercepts were compared with a Student t-test. In the absence of significant differences between the slopes of CC9 and CC29 (t = 1.01; df = 652; *p>0.05*) and their y-intercepts (t = 1.71; df = 652; *p>0.05*), a general temperature equation, representative of the these two *C. compactum* specimens, was calculated for the time interval of 1975 to 2015 (R^2 = 0.61; N = 656):

$$SST = 0.37(Mg/Ca(mmol/mol))-40.39 \quad (3)$$

Due to the shift in Mg/Ca values between CC25 and the two other specimens (Figure 6), significant differences were obtained between the slopes and the y-intercepts of the latter and CC9 or CC29 (t > 8.00; df = 652; *p<0.05* in all comparisons). Hence, it is impossible to take CC25 into account for the calculation of the general equation and this is valid only for the determination of that equation. However, for the comparisons with environmental parameters, we averaged the Mg/Ca time-series of the three specimens. Thus, a significant and positive correlation was found between monthly Mg/Ca values and monthly SST measured at station 27 (r = +0.75; *p<0.05*). Similary, a significant positive relationship was found between Ba/Ca time-series and monthly values of the Tail of the Grand Bank Labrador Current transport over the period 1993-2013 (r = +0.33; *p<0.05*). Finally, Ba/Ca values were significantly correlated with surface salinities recorded at station 27 (r = +0.31; *p<0.05*).

Lastly, to compare our growth and geochemical data with sea water temperatures, we used two different databases. We proceeded this way because the NOAA-NODC database has a smaller spatial resolution and is less dependent on the cloud cover while the NOAA_ERSST_v4 dataset allows the extraction of SST values around SPM in order to compare data at a more local scale. Moreover, the NOAA-NODC database is an average of the ocean temperature between the surface

and 100 m water depth. This latter feature allows a better characterization of water masses and is more relevant for our large-scale spatial correlations. Nonetheless, as an indication, we calculated spatial correlations between SGI_{direct} and the NOAA_ERSST_v4 satellite-based SST and found very similar results than those presented in Figure 8.

4. Discussion

4.1. Growth analyses

4.1.1. Use of Mutvei's solution to reveal growth lines

To our knowledge, this is the first time that Mutvei's solution staining was tested on coralline red algae in order to reveal periodic growth lines. This study demonstrated that this method is effective and allows direct increment width measurements on *C. compactum* carbonate structures (Fig 2C, D). Here, *C. compactum* cross-sections treated with Mutvei's solution revealed annual growth lines characterized by distinct, darker blue colored lines. The main advantages of this technique are (i) its rapidity and (ii) its low cost compared to micro-chemical analyses. In addition, Mutvei's solution may also yield important clues to *C. compactum* growth and biomineralization processes. For example, our results showed that growth lines are more strongly stained and etch-resistant than growth increments, confirming that fast growth periods of *C. compactum* are associated with larger and less calcified cells, while smaller and more calcified cells form in winter during slow growth (Moberly, 1968; Halfar et al., 2008). Nonetheless, it appeared that growth lines could merge or disappear, mostly in the youngest part of cross-sections. This can be due to morphological features that only occur in some portions of algae hard structures or to external factors that will be discussed in the next paragraph. However, growth lines were certainly visible and could be pinpointed, but this issue made backdating based on direct measurements very uncertain or even impossible in most specimens. That is the reason why all of them (including CC9 and CC25) were not taken into account in the SGI_{direct} master-chronology. Moreover, even if Schöne et al. (2017) showed no isotope (carbon and oxygen) changes after soaking carbonates in Mutvei's

solution, it still needs to be tested which elements are affected by Mutvei's solution. That is why we decided to perform our geochemical analyses on carbonate samples that underwent minimal pre-treatments. In this study, *C. compactum* slices used for geochemical analyses were soaked in Mutvei's solution only after LA-ICP-MS measurements.

When comparing the two SGIs master-chronologies contructed via direct and indirect reading methods, we found that they were positively and significatively correlated with each other. This result suggested that the variability in growth signals is similar whatever the measurement method. However, it appears that indirect measurements could lead to an overestimation of annual increment width likely due to the laser paths which were not always perfectly parallel to the direction of growth (i.e. perpendicular to annual growth lines). Moreover, the positions of growth marks do not perfectly fit to the minimum values of Mg/Ca (Figure 6A). Nonetheless, the configuration of this study and the geochemical analyses we undertook do not allow an optimal comparison between these two methods and further studies could focus on increasing the number of studied algae and especially in analyzing the growth signals extracted from the same specimens with both methods. This new experimental design could quantify the impacts of growth measurements methods on the comparisons with environmental parameters. We will therefore discuss the results from direct growth line measurements (SGI_{direct}) until the rest of the paper.

4.1.2. Growth signal interpretation

Based on direct growth measurements, average growth rate of all specimens was 248 µm ($\pm$ 69 µm). This is consistent with previous reports on the annual growth rate of *C. compactum* from the Northwest Atlantic (Adey, 1965; Halfar et al., 2011; Adey et al., 2013; Williams et al. 2018). Successful cross dating of annual increments is a key to evaluate if individuals are consistently responding to common external factors (Douglas, 1920). This study demonstrated that this is the case for *C. compactum* from SPM (inter-series correlation = 0.33). This value is fully

comparable with those from other dendrochronological studies (Black et al. 2010) although it is lower than values usually obtained with other biotas such as *Arctica islandica* (e.g. Butler et al., 2013), or the Tuliptree *Liriodendron tulipifera* (e.g. Wilde & Maxwell, 2018). This relatively low inter-series correlation value combined with intra-individual variability of annual increment widths reveal the existence of difficulties associated with the use of *C. compactum* growth as an environmental proxy. Several studies have shown that *C. compactum* growth is predominantly governed by light and temperature (e.g. Halfar et al. 2011; Adey et al. 2013). However, quantification of growth parameters remains a complex issue. This is related to the nature of this biological response (growth) which integrates a multitude of environmental parameters whether biotic (e.g. predation) or abiotic (e.g. light availability, pollution), in varying proportions over time. In addition, these environmental conditions can be highly variable among and within specimens. For example, shading, predation, disease, or grow-out from damaged postmature conceptacles can change *C. compactum* growth and geochemical composition (Adey et al., 2013). In this study, *C. compactum* specimens were subject to grazing activities by sea urchins (Steneck, 1986) making most of them unreadable for sclerochronological analyses. Usually, these grazing tracks are easily observable after the cutting step allowing a first quality control of the samples and thus, the removal of some specimens from analyses. However, a slight grazing, like those made by chitons (Steneck, 1992), is hardly observable and can results in smaller increment widths and lead to unreliable growth information. Light conditions can also affect *C. compactum* growth rate (Adey, 1970) and are highly variable down to the specimen level, according to its position and shading provided by macroalgal cover. As mentioned above, these external factors affecting annual growth rates are not necessarily stable on a multidecadal time scale. Nonetheless, the shading impacts can be limited by increasing the amount of *C. compactum* sampling sites, while variability of growth among conspecific specimens can be reduced by combining growth record of different transects (Halfar et al., 2011).

4.2. Geochemical analyses

First of all, we will discuss the way in which chemical analyses were performed. According to previous reports, matrix effects of LA-ICP-MS can result in chemical differences of up to 10% between measurements on different days (Hetzinger et al., 2011; Williams et al., 2014). This may partially explain the higher Mg/Ca and lower Ba/Ca baselines observed in specimen CC25 than in CC9 – CC29, which were measured 15 days earlier. Another explanation for this deviation would be that the inclusion of these trace elements into carbonate matrix of the algae varies among specimens within a population. This is likely due to different light exposures that can drive this incorporation process (Adey et al., 1970; Williams et al., 2018; see also a more elaborated discussion below). Moreover, Nash et al. (2019) demonstrate that the Mg content of *Clathromorphum spp.* could differ between specimens and is dependent of the cell wall layout type. While specimens of this genus have a Mg content that commonly ranges from 7.4 to 16.9 %mol of $MgCO_3$ (noted M-type), some rare specimens have a naturally higher Mg content. Within this so-called D-type specimens, the Mg content recorded into *Clathromorphum spp.* cell walls ranges from 25 to 36 %mol of $MgCO_3$. However, this gap, which results in a significantly different linear regression, led us to exclude the CC25 specimen from the SST calibration with magnesium distribution. Moreover, our choice is supported by the Mg/Ca ratios measured within *C. compactum* and used so far in sclerochronological studies which are of the same order of magnitude as CC9 and CC29 Mg/Ca values (e.g. Williams et al., 2014; Hetzinger et al., 2018). Nonetheless, it would have been necessary to analyze a larger amount of specimens in order to increase the robustness of the calibration and to provide a detailed explanation of the measured deviation in magnesium and barium concentrations of CC25. This analytical uncertainty, however, does not explain the interannual variability between transects or between specimens. Furthermore, the choice of calcium as internal standard could also be a source of bias. The calcium distribution may not be constant within the hard structures of coralline red algae. Thus, expressing coralline red algae

micro-chemical results as element-to-calcium ratios could affect geochemical data. However, the heterogeneous distribution of calcium within calcite matrix of coralline algae still needs to be confirmed through other analytical techniques.

In order to be considered as an environmental proxy, trace element time-series must follow the same trends along several transects within an entire specimen and within a population. In this study, intra-specimen variability was assessed for Mg/Ca and Ba/Ca by comparing pairs of transects using Spearman's rank correlation coefficients (Figure 7). All Mg/Ca series were significantly correlated to each other, with only one exception (transects T3 and T4 for CC29). The values of these coefficients were variable, ranging from 0.08 to 0.67. Similar observations were done for Ba/Ca, for which 32 out of 36 series were significantly correlated (r values ranging between 0.06 and 0.47). These results indicate the presence of differences among specimens, an aspect that has been discussed in previous studies (e.g. Gamboa, 2010; Williams et al., 2014; Hetzinger et al., 2018; Williams et al., 2018). One proposed explanation is based on laser ablation transects positions. As replicated transects are not necessarily perfectly parallel with direction of growth at all times due to the avoidance of conceptacles, then each LA-ICP-MS data point will represent different time intervals. Another explanation is related to LA-ICP-MS measurements, which may capture microstructural and chemical features in some parts of cross-sections and not in others. This may reflect biological processes altering geochemistry properties during calcification (e.g. predation, disease, grow-out from damaged postmature conceptacles). The other issue is related to inter-specimen variability. This has been tested by comparing averaged Mg/Ca and Ba/Ca time-series of different specimens using Spearman's rank correlation coefficients. The values of these correlation coefficients were higher than those obtained for transects within the same specimen, ranging from 0.77 to 0.79 for Mg/Ca and 0.65 to 0.69 for Ba/Ca. This result suggests that chemical variability within specimen is fully comparable among different specimens. To conclude, our findings agree with previous reports and demonstrate that calculating sample composites from

multiple sampling transects per specimen decreases analytical noise (e.g. Gamboa, 2010; Hetzinger et al., 2011; Williams et al., 2014; Hetzinger et al. 2018; Williams et al., 2018).

Since we have discussed analytical biases related to geochemical measurements performed in this study, we will now focus on Mg/Ca and Ba/Ca as potential environmental proxies. Several studies pointed out that skeletal Mg/Ca variations in *Clathromorphum sp.* are related to temperature (Hetzinger et al., 2009; Gamboa, 2010; Halfar et al., 2008; Hetzinger et al., 2018; Williams et al., 2018) and display seasonal cyclicity (Adey et al., 2013). However, pioneer studies also evidence that light influences Mg incorporation into coralline red algae (Moberly, 1968; Adey, 1970). More recently, Williams et al. (2018) demonstrated that both light and temperature significantly affect Mg incorporation into *C. compactum* calcite matrix. Based on experiments carried out in controlled environment, they also pointed out that, at lower temperatures the effects of light are slightly smaller than at higher temperature (Adey, 1970). Following these findings, Mg/Ca-based temperature reconstructions with *Clathromorphum sp.* require site-specific temperature calibrations that consider local light conditions. Therefore, we performed a linear regression analyses between Mg/Ca ratio and SST. From our results, moderate linear correlation (R^2 = 0.61) exists between Mg/Ca and SST suggesting that Mg/Ca variability at SPM is not fully explained by satellite-based SST. The reason for this would be that satellite data used in this study might not accurately capture bottom temperatures experienced by the coralline algae from SPM, where the hydrological environment is highly variable below the surface. Indeed, *in situ* temperature from the SPM setting where the coralline algae samples were collected is influenced by coastal trapped waves which do not influence satellite-based SST (Bezaud et al., 2017; Bezaud et al., 2018; Lazure et al., 2018). However, the lack of long-term temperature records from our study site required the use of these SST satellite-based measurements. Since instrumental records of past light variability are limited, we could not quantify its influence on geochemical composition of coralline red algae. Thus, we followed the recommendations by Williams et al. (2018) and

averaged all geochemical data to create one single time-series for each elemental ratio. This method was applied to prevent outliers, that may have experienced significantly different light levels, from having an effect on the proxy reconstruction. Moreover, averaging time-series can also reduce the effect that individual morphological characteristics can have on geochemical data (Nash et al., 2019). The environmental analyses, presented in the next section, will therefore be based on an average of the twenty seven Mg/Ca time-series.

Previously, Ba/Ca in coralline red algae have been used for coastal runoff reconstruction (Chan et al., 2011), stratification, and/or upwelling depending on barium sources, which can be terrigenous (from freshwater inputs) or biogenic (from phytoplankton bloom), in surface waters (Hetzinger et al., 2013). In a recent study performed in the Northwest Atlantic Ocean, Chan et al. (2017) proposed to interpret Ba/Ca from *C. compactum* as a primary productivity signal. This assumption is based on barium availability in the LC, determined by biological scavenging due to phytoplankton efflorescences, and the variability of its influence on water masses surrounding *C. compactum* through time. Nonetheless, recent sclerochronological studies based on *C. compactum* tend to demonstrate that barium signal interpretation as an environmental proxy seems to be site specific and dependent of the barium sources (Chan et al., 2011; Hetzinger et al., 2013; Chan et al., 2017). That is why further studies need to be conducted in SPM in order to clearly identify barium sources and refine our interpretation of this geochemical signal recorded within *C. compactum* calcitic structure. Based on the same reasons given previously for magnesium, environmental analyses presented in the next section are based on an average of the twenty-seven Ba/Ca time-series.

To conclude this section, we would like to focus on the correlations we obtained between geochemical data recorded within *C. compactum* calcitic matrix and environmental conditions. It is important to note that calculate correlations based on monthly time-series could lead to a bias due

to annual cycles that might drive these autocorrelations. Nonetheless, when averaging monthly values in order to obtain annual data, the calculated correlations were weaker and not significant. The reason for this would be that growth of *C. compactum* is not constant throughout one year (Halfar et al., 2011). Thus, the inclusion of trace elements into specimens hard strucutres is dependent of the month and it is therefore necessary to weight these averages according to the monthly growth rates, which cannot be done here. However, correlating monthly data seems to be the method commonly used so far in order to compare geochemical signals and environmental parameters (Kamenos et al., 2012; Williams et al., 2014; Hetzinger et al., 2018).

4.3. Environmental reconstruction in the Northwest Atlantic region

Recent studies based on *Arctica islandica* paleoenvironmental records from SPM archipelago pointed out the importance to consider multi-scale hydro-climatic forcing and interactions to understand local ecological processes (Poitevin et al., 2019; Doré et al., 2020). Based on this observation, we will discuss environmental implications of our *C. compactum* sclerochronological and geochemical results at regional and large scales.

First, we sought relationships between *C. compactum* growth at SPM and large-scale climatic indices (AMO, NAO and AO). These drivers strongly influence marine ecosystem structure (Carroll et al., 2014; Poitevin et al., 2019; Doré et al., 2020) at decadal or multi-decadal time scales. At SPM, only the AMO was positively and significantly correlated with *C. compactum* annual growth variability. While a longer growth time-series might provide more robust comparisons, these results indicate that part of *C. compactum* growth variability may be explained by near-surface temperature over the North Atlantic, which is consistent with positive spatial correlations between *C. compactum* SGI from SPM and temperature within the Sub Polar Gyre (SPG) extent (Figure 8). These highlights led us to further explore SPG dynamics and its influence on water properties around SPM. The significant negative correlation obtained between *C. compactum*

growth rates in SPM and the SPG index seems to have the same interpretation as temperature spatial correlations and raises questions of global scale influence on local ecological processes. These implications have previously been discussed in several studies based on *C. compactum* paleoenvironmental records from the same region (Chan et al., 2017) and on *A. islandica* from SPM archipelago (Poitevin et al., 2019; Doré et al., 2020). The latter studies pointed towards the same directions as ours and showed that global scale hydro-climatic processes affect LC nutrient availability and its influence on Newfoundland coastal ecosystems. Based on these assumptions, we compared our proxy records to regional environmental datasets to get insights about LC dynamics and its influence on SPM coastal ecosystems.

The LC flows toward the equator and carries cold and less saline water of Arctic origin along the Labrador slope and Grand Banks, finally affecting the whole Middle Atlantic Bight (e.g., Chapman & Beardsley, 1989) (Figure 1). The spatiotemporal structure of the LC along the Labrador coasts and over the Grand Banks is complex. On the Newfoundland shelf, it has two branches: (i) a main offshore branch flowing south and feeding the North Atlantic Current, and (ii) a smaller inshore branch that flows over the Labrador shelf and spreads along the Newfoundland coast over the Grand Banks with flow rates ten times weaker (Petrie & Anderson, 1983; Lazier & Wright, 1993). This led us to further investigate the LC inshore branch dynamics and its influence on *C. compactum* at SPM. Station 27 located in the Avalon channel within the LC inshore branch provides the longest SST and sea surface salinity (SSS) time-series in this area. Strong positive correlations were found between magnesium and barium concentrations in calcified structures of *C. compactum* from SPM and station 27 SST and SSS, respectively. Hetzinger et al. (2013) found the same significant relationships between Ba/Ca series of *C. compactum* from Eastern Newfoundland coastal waters (also influenced by LC inner branch) and recorded salinity at station 27. Nonehteless, the physical dynamics of the LC remains to be addressed. In this way, the Grand Banks could affect the SPM region under certain conditions (Peterson et al., 2017; Petrie &

Drinkwater, 1993; Poitevin et al., 2019). A part of the offshore branch of LC that follows the continental slope retroflexes to the east, joining the North Atlantic Current (Figure 1) before reaching the tail end of the Grand Banks (Fratantoni & McCartney, 2009). The remaining LC branch flows westward after the tail of Grand Banks and turns northward, toward Cabot Strait and may spread around the SPM region (Petrie & Anderson, 1983; Urrego-Blanco & Sheng, 2014; Poitevin et al., 2019). This transport at the tail end of Grand Bank was calculated for 1992 to 2013 and correlate positively with SPM *C. compactum* Ba/Ca variations which has previously been reported as a primary productivity signal (Chan et al., 2017).

Our results are in accordance with those obtained by several paleoenvironmental studies from the same region (Chan et al., 2017; Poitevin et al., 2019; Doré et al., 2020) and tend to confirm the relevance of scientific research carried out along SPM to study large-scale oceanographic variability and its implication on coastal ecosystem dynamics facing global changes.

5. Conclusions and Perspectives

This study demonstrates that direct growth measurements after Mutvei solution staining were equally effective and less expensive than indirect growth measurement based on geochemical analyses. Advantages related to this new method should enhance the number of studied specimens in coralline red algae growth studies, thereby limiting uncertainties related to intra- and inter-specimen variabilities. Moreover, the use of a standard method amongst species or biological taxa pave the way for larger-scale comparison and more accurate paleoenvironmental reconstructions. Furthermore, because of the high reproducibility of Mg/Ca and Ba/Ca time-series within a single individual and among several specimens, this study confirmed the use of both trace elements for environmental investigations. Geochemical information, combined with growth analyses, enhanced our understanding of hydro-climatic variabilities around SPM and ocean dynamics in the Northwest Atlantic region. The strong consistency between environmental

information obtained from this study and other sclerochronological ones from the same region, which used other biotas (Chan et al., 2017; Poitevin et al., 2019; Doré et al., 2020), demonstrates the relevance of starting multi-proxy reconstructions in this area. The main advantage of this kind of approach is that each archive records climate variability from its unique “perspective” of habitat, location, life history, or trophic level such that their combination yields a more holistic perspective of the past environmental changes than any data set could provide on its own (Black et al., 2009). This is particularly true for regions, such as SPM archipelago, where complex multi-scale hydro-climatic interactions influence coastal ecosystem dynamics.

Acknowledgements

We thank Anne-Sophie Podeur, Geneviève Cohat and Yves Larsonneur, the LEMAR (UMR 6539) Secretariat team, for their assistance during the administrative preparation of the field trip. We kindly acknowledge Yoann Busnot, Luc Thillais and Jean-Marc Derouetk, from the DTAM divers’crew, for their help during the sampling of *C. compactum* specimens. We are sincerely grateful to the Club Nautique Saint-Pierrais and its president, Stephane Salvat, for renting their boat, for their kindness and availability. In addition, we express our sincere gratitude to Herlé Goraguer (IFREMER) for his invaluable help with local authorisations and logistics. We are also grateful to Bleuenn Gueguen and Marie-Laure Rouget, from the “Pôle Spectrométrie Océan (PSO)”, who helped us with the LA-ICP-MS analyses. Finally, we express our sincere appreciation to Philippe Eliès from the ''Plateforme d'Imagerie et de Mesures en Microscopie (PIMM)'' of the University of Western Brittany for his support with SEM imageing. This work was supported by the EC2CO program MATISSE of the CNRS INSU, the Cluster of Excellence LabexMER, the European Institute for Marine Studies (IUEM) and the LIA BeBEST CNRS INEE.

References

Adey W. H. (1965). The genus Clathromorphum (Corallinaceae) in the Gulf of Maine. *Hydrobiologia*, *26*(3–4), 539–573. https://doi.org/10.1007/BF00045545

Adey, W. H. (1970). The effects of light and temperature on growth rates in boreal-subarctic crustose corallines. *Journal of Phycology*, *6*(3), 269-276

Adey, W. H., Halfar, J., & Williams, B. (2013). *The coralline genus Clathromorphum foslie emend. adey: biological, physiological, and ecological factors controlling carbonate production in an arctic-subarctic climate archive*.

Berx B., & Payne M. R. (2017). The Sub-Polar Gyre Index - A community data set for application in fisheries and environment research. *Earth System Science Data*, *9*(1), 259–266. https://doi.org/10.5194/essd-9-259-2017

Bezaud, M., Lazure, P., & Le Cann, B. (2017). Barotropic Hydrodynamics at high Frequency around the archipelago of Saint Pierre and Miquelon. *EGUGA*, 14709.

Bezaud, M., Lazure, P., & Le Cann, B. (2018). Hydrodynamics at high frequency around the archipelago of Saint Pierre and Miquelon. *EGUGA*, 14970.

Black B. A., Shaw D. C., & Stone J. K. (2010). Impacts of Swiss needle cast on overstory Douglas-fir forests of the western Oregon Coast Range. *Forest Ecology and Management*, *259*(8), 1673–1680. https://doi.org/10.1016/j.foreco.2010.01.047

Black B. A, Copenheaver C. A., Frank D. C., Stuckey M. J., & Kormanyos R. E. (2009) Multi-proxy reconstructions of northeastern Pacific sea surface temperature data from trees and Pacific geoduck. *Palaeogeography, Palaeoclimatology, Palaeoecology*, *278*, 40–47. https://doi.org/10.1016/j.palaeo.2009.04.010

Bunn, A. G. (2008). A dendrochronology program library in R (dplR). Dendrochronologia 26, 115–124. doi: 10.1016/j.dendro.2008.01.002

Butler P. G., Wanamaker A. D., Scourse J. D., Richardson C. A., & Reynolds D. J. (2013). Variability of marine climate on the North Icelandic Shelf in a 1357-year proxy archive based on growth increments in the bivalve Arctica islandica. *Palaeogeography, Palaeoclimatology, Palaeoecology*, *373*, 141–151. https://doi.org/10.1016/j.palaeo.2012.01.016

Carroll M. L. , Ambrose W. G. Jr., Locke W.L. , Ryan S.K., & Johnson B.J. (2014) Bivalve growth rate and isotopic variability across the Barents Sea Polar Front. *Journal of Marine Systems*, *130*, 167–180.

Chan P., Halfar J., Williams B., Hetzinger S., Steneck R., Zack T., & Jacob D. E. (2011). Freshening of the Alaska Coastal Current recorded by coralline algal Ba/Ca ratios. *Journal of Geophysical Research: Biogeosciences*, *116*(1), 1–8. https://doi.org/10.1029/2010JG001548

Chan, P., Halfar, J., Adey, W., Hetzinger, S., Zack, T., Moore, G. W. K., ... & Hou, A. (2017). Multicentennial record of Labrador Sea primary productivity and sea-ice variability archived in coralline algal barium. *Nature communications*, *8*(1), 1-10.

Chapman D.C., & Beardsley R.C. (1989) On the origin of shelf water in the Middle Atlantic Bight. *Journal of Physical Oceanography*, *19*, 384–391.

Chave K. E. (1954). Aspects of the Biogeochemistry of Magnesium 1. Calcareous Marine Organisms. *The Journal of Geology*, *62*(3), 266–283. https://doi.org/10.1086/626162

Doré, J., Chaillou G., Poitevin, P., Lazur, P., Poirié, A., Chauvaud, L., ... & Thébault, J., (2020). Assessment of Ba/Ca in Arctica islandica shells as a proxy for phytoplankton dynamics in the Northwestern Atlantic Ocean. *Estuarine, Coastal and Shelf Science*, *237*, 106628.

Dahlgren, T. G., Weinberg, J. R., & Halanych, K. M. (2000). Phylogeography of the ocean quahog (Arctica islandica): influences of paleoclimate on genetic diversity and species range. *Marine Biology*, *137*(3), 487-495.

Douglas AE (1920) Evidence of climatic effects in the annual rings of trees. *Ecology*, *1*, 24-27.

Dunbar B., Wellington M., Colgan W., & Glynn P. W. (1994). Eastern Pacific sea surface temperature since 1600 A.D.: The record of climate variability in Galápagos corals. *Paleobiology*, *9*(2), 291–315. https://doi.org/10.1029/93PA03501

Fratantoni P. S., & McCartney M.S. (2009) Freshwater export from the Labrador Current to the North Atlantic Current at the Tail of the Grand Banks of Newfoundland. *Deep-Sea Research I, 57*, 258–283.

Gamboa, G. (2010). *Mg/Ca Ratios in Crustose Coralline Algae as Proxies for Reconstructing Labrador Current Variability* (Doctoral dissertation).

Goodwin D. H., Schöne B. R., & Dettman D. L. (2009). Resolution and Fidelity of Oxygen Isotopes as Paleotemperature Proxies in Bivalve Mollusk Shells: Models and Observations. *Palaios*, *18*(2), 110–125.

Grissino-Mayer, H. D. (2001). Evaluating crossdating accuracy: a manual and tutorial for the computer program COFECHA. Tree-Ring Res. 57, 205–221

Halfar J., Adey W. H., Kronz A., Hetzinger S., Edinger E., & Fitzhugh W. W. (2013). Arctic sea-ice decline archived by multicentury annual-resolution record from crustose coralline algal proxy. *Proceedings of the National Academy of Sciences*, *110*(49), 19737–19741. https://doi.org/10.1073/pnas.1313775110

Halfar J., Hetzinger S., Adey W., Zack T., Gamboa G., Kunz B., Williams B., & Jacob D. E. (2011). Coralline algal growth-increment widths archive North Atlantic climate variability. *Palaeogeography, Palaeoclimatology, Palaeoecology*, *302*(1), 71–80. https://doi.org/10.1016/j.palaeo.2010.04.009

Halfar J., Steneck R. S., Joachimski M., Kronz A., & Wanamaker A. D. (2008). Coralline red algae as high-resolution climate recorders. *Geology*, *36*(6), 463–466. https://doi.org/10.1130/G24635A.1

Hetzinger S., Halfar J., Kronz A., Simon K., Adey W. H., & Steneck R. S. (2018). Reproducibility of Clathromorphum compactum coralline algal Mg/Ca ratios and comparison to high-resolution sea surface temperature data. *Geochimica et Cosmochimica Acta*, *220*, 96–109. https://doi.org/10.1016/j.gca.2017.09.044

Hetzinger S., Halfar J., Kronz A., Steneck R. S., Adey W. H., Lebednik P. A., & Schöne B. R. (2009). High-Resolution Mg/Ca Ratios in a Coralline Red Alga As a Proxy for Bering Sea Temperature Variations From 1902 To 1967. *Palaios*, *24*(6), 406–412. https://doi.org/10.2110/palo.2008.p08-116r

Hetzinger S., Halfar J., Zack T., Gamboa G., Jacob D. E., Kunz B. E., … Steneck R. S. (2011). High-resolution analysis of trace elements in crustose coralline algae from the North Atlantic and North Pacific by laser ablation ICP-MS. *Palaeogeography, Palaeoclimatology, Palaeoecology*, *302*, 81–94. https://doi.org/10.1016/j.palaeo.2010.06.004

Hetzinger S., Halfar J., Zack T., Mecking J. V., Kunz B. E., Jacob D. E., & Adey W. H. (2013). Coralline algal Barium as indicator for 20th century northwestern North Atlantic surface ocean freshwater variability. *Scientific Reports*, *3*, 1–8. https://doi.org/10.1038/srep01761

Hetzinger, S., Halfar, J., Zajacz, Z., & Wisshak, M. (2019). Early start of 20th-century Arctic sea-ice decline recorded in Svalbard coralline algae. *Geology*, *47*(10), 963-967.

Hurrell J. W., Kushnir Y., & Visbeck M. H. (2001). The North Atlantic Oscillation. *Science*, *291*(5504), 603–5. https://doi.org/10.1126/science.1058761

Jochum K.P., Nohl U., Herwig K., Lammel E., Stoll B., Hofmann A.W. (2005). GeoReM: A new geochemical database for reference materials and isotopic standards. Geostandards and Geoanalytical Research 29(3): 333-338

Kamenos N. A., Cusack M., & Moore P. G. (2008). Coralline algae are global palaeothermometers with bi-weekly resolution. *Geochimica et Cosmochimica Acta*, *72*(3), 771–779. https://doi.org/10.1016/j.gca.2007.11.019

Kamenos N. A., Hoey T. B., Nienow P., Fallick A. E. and Claverie T. (2012) Reconstructing Greenland ice sheet runoff using coralline algae. Geology 40, 1095–1098.

Knight J. R., Folland C. K., & Scaife A. A. (2006). Climate impacts of the Atlantic multidecadal oscillation. *Geophysical Research Letters*, *33*(17), 2–5. https://doi.org/10.1029/2006GL026242

Lazier, J. R., & Wright, D. G. (1993). Annual velocity variations in the Labrador Current. *Journal of Physical Oceanography*, *23*(4), 659-678.

Lazure, P., Le Cann, B., & Bezaud, M. (2018). Large diurnal bottom temperature oscillations around the Saint Pierre and Miquelon archipelago. *Scientific reports*, *8*(1), 1-12.

Lewis, B., & Diaz-Pulido, G. (2017). Suitability of three fluorochrome markers for obtaining in situ growth rates of coralline algae. *Journal of Experimental Marine Biology and Ecology*, *490*, 64-73.

Moberly Jr. R. (1968). Composition of magnesian calcites of algae and pelecypods by electron microproe analysis. *Sedimentology*, *11*, 61–82.

Moore, G. W. K., Halfar, J., Majeed, H., Adey, W., & Kronz, A. (2017). Amplification of the Atlantic Multidecadal Oscillation associated with the onset of the industrial-era warming. *Scientific reports*, *7*(1), 1-10.

Nash, M. C., Diaz-Pulido, G., Harvey, A. S., & Adey, W. (2019). Coralline algal calcification: A morphological and process-based understanding. *PloS one*, *14*(9), e0221396.

Poitevin, P., Thebault, J., Siebert, V., Donnet, S., Archambault, P., Doré, J., ... & Lazure, P. (2019). Growth response of Arctica islandica to North Atlantic oceanographic conditions since 1850. *Frontiers in Marine Science*, *6*, 483.

Paillard D., Labeyrie L., & Yiou P. (1996). AnalySeries 1.0: a Macintosh software for the analysis of geophysical time-series. *Eos*, *77*, 379.

Peterson I., Greenan B., Gilbert D., Hebert D. (2017) Variability and wind forcing of ocean temperature and thermal fronts in the Slope Water region of the Northwest Atlantic. *Journal of Geophysical Research Oceans, 122*, 7325–7343.

Petrie B., & Anderson C. (1983) Circulation on the Newfoundland Continental Shelf. *Atmosphere-Ocean, 21 (2)*, 207–226.

Petrie B., & Drinkwater K. (1993) Temperature and salinity variability on the Scotian Shelf and in the Gulf of Maine 1945-1990. *Journal of Geophysical Research-Oceans and Atmospheres*, *98*, 20079–20089.

Rahmstorf S. (2003). The current climate. *Nature*, *421*(6924), 699. https://doi.org/10.1038/421699a

Saenger C., Cohen A. L., Oppo D. W., Halley R. B., & Carilli J. E. (2009). Surface-temperature trends and variability in the low-latitude North Atlantic since 1552. *Nature Geoscience*, *2*(7), 492–495. https://doi.org/10.1038/ngeo552

Schöne B. R. (2013). Arctica islandica (Bivalvia): A unique paleoenvironmental archive of the northern North Atlantic Ocean. *Global and Planetary Change*, *111*, 199–225. https://doi.org/10.1016/j.gloplacha.2013.09.013

Schöne B. R., Dunca E., Fiebig J., & Pfeiffer M. (2005). Mutvei's solution: An ideal agent for resolving microgrowth structures of biogenic carbonates. *Palaeogeography, Palaeoclimatology, Palaeoecology*, *228*(1–2), 149–166. https://doi.org/10.1016/j.palaeo.2005.03.054

Schöne B. R., Schmitt K., & Maus M. (2017). Effects of sample pretreatment and external contamination on bivalve shell and Carrara marble δ18O and δ13C signatures. *Palaeogeography, Palaeoclimatology, Palaeoecology*, *484*, 22–32. https://doi.org/10.1016/j.palaeo.2016.10.026

Sirot C., Ferraton F., Panfili J., Childs A. R., Guilhaumon F., & Darnaude A. M. (2017). Elementr: An R package for reducing elemental data from LA-ICPMS analysis of biological calcified structures. *Methods in Ecology and Evolution*, *8*(12), 1659–1667. https://doi.org/10.1111/2041-210X.12822

Sletten H. R., Andrus C. F. T., Guzmán H. M., & Halfar J. (2017). Re-evaluation of using rhodolith growth patterns for paleoenvironmental reconstruction: An example from the Gulf of Panama. *Palaeogeography, Palaeoclimatology, Palaeoecology*, *465*, 264–277. https://doi.org/10.1016/j.palaeo.2016.10.038

Steneck R. S. (1986). The Ecology of Coralline Algal Crusts : Convergent Patterns and Adaptative Strategies. *Annual Review of Ecology and Systematics*, *17*, 273–303.

Steneck, R. S. (1992). Plant-herbivore coevolution: a reappraisal from the marine realm and its fossil record. *Plant-animal interactions in the marine benthos*, 477-91.

Thompson D. W. J., & Wallace J. M. (1998). The Arctic Oscillation signature in the wintertime geopotential height and temperatuer field. *Geophysical Research Letters*, *25*(9), 1297–1300.

Urrego-Blanco J., & Sheng J. (2014) Study on subtidal circulation and variability in the Gulf of St. Lawrence, Scotian Shelf, and Gulf of Maine using a nested-grid shelf circulation model. *Ocean Dynamics*, *64*, 385–412.

Wanamaker A. D., Kreutz K. J., Schöne. B. R., Pettigrew N., Borns H. W., Introne D. S., … Feindel S. (2008). Coupled North Atlantic slope water forcing on gulf of Maine temperatures over the past millennium. *Climate Dynamics*, *31*, 183–194. https://doi.org/10.1007/s00382-007-0344-8

Wanner, H., Brönnimann, S., Casty, C., Gyalistras, D., Luterbacher, J., Schmutz, C., ... & Xoplaki, E. (2001). North Atlantic Oscillation–concepts and studies. *Surveys in geophysics*, *22*(4), 321-381. doi: 10.1023/A:1014217317898

Wilde E. M., & Maxwell J. T. (2018). Comparing climate-growth responses of urban and non-urban forests using L. tulipifera tree-rings in southern Indiana, USA. *Urban Forestry and Urban Greening*, *31*, 103–108. https://doi.org/10.1016/j.ufug.2018.01.003

Williams B., Halfar J., Steneck R. S., Wortmann U. G., Hetzinger S., Adey W. H., … Joachimski M. (2011). Twentieth century δ13C variability in surface water dissolved inorganic carbon recorded by coralline algae in the northern North Pacific Ocean and the Bering Sea. *Biogeosciences*, *8*(1), 165–174. https://doi.org/10.5194/bg-8-165-2011

Williams, B., Halfar, J., DeLong, K. L., Hetzinger, S., Steneck, R. S., & Jacob, D. E. (2014). Multi-specimen and multi-site calibration of Aleutian coralline algal Mg/Ca to sea surface temperature. *Geochimica et Cosmochimica Acta*, *139*, 190-204.

Williams S., Halfar J., Zack T., Hetzinger S., Blicher M., & Juul-Pedersen T. (2018). Comparison of climate signals obtained from encrusting and free-living rhodolith coralline algae. *Chemical Geology*, *476*, 418–428. https://doi.org/10.1016/j.chemgeo.2017.11.038

Wu Y., Tang C., & Hannah C. (2012). The circulation of eastern Canadian seas. *Progress in Oceanography*, *106*, 28–48.

Figure captions

Figure 1: (A) Major features of the regional surface circulation (inspired by Fig.1 in Poitevin et al., 2019) with main location names and bathymetry lines. The cold inshore and offshore Labrador currents are in blue; Gulf Stream and North Atlantic currents are in red. In green is historical hydrographic Station 27 (Stn 27). The main acronyms corresponding to location names are as follows: NL – Newfoundland; SPB – Saint-Pierre Bank; GSL – Gulf of Saint-Lawrence; AC – Avalon Channel; and GB – Grand Banks. (B) Sampling location of *Clathromorphum compactum* (red dot).

Figure 2: Steps of sample preparation with (A) a lateral view from side and (B) an axial view from top of one specimen showing the three different cutting axes (red lines). Thick blue line (slice 1) corresponds to the 2mm thick section stained with Mutvei's solution for growth analyses and thick white lines (slices 2, 3, 4) represent the cross-sections dedicated to geochemical analysis. (C) A cross-section before and after Mutvei's solution staining, facilitating growth measures. (D) Enlarged image showing growth increment measurements. (E) SEM photograph of one growth line after Mutvei's solution treatment.

Figure 3: (A) Picture of one cross-section (slice 2) dedicated to geochemical analyses showing the positions and labels of laser ablation transects. On slices 3 and 4, transects are labeled T4, T5, T6 and T7, T8, T9 respecively. (B) Portion of a cross-section coloured with Mutvei's solution after LA-ICP-MS analyses.

Figure 4: Intra-specimen variability of annual increment widths directly measure among the seven studied specimens. Values in boxes are Spearman's correlation coefficients, crossed-out numbers were non-significant at $p<0.05$.

Figure 5: (A) Lifespan of the collected specimens used in constructing the SGI_{direct} master-chronology on the left side. On the right side are the *C. compactum* individual growth time-series (grey curves) and SGI_{direct} master-chronology (black curve). (B) Lifespan of each specimen used in constructing the $SGI_{indirect}$ master-chronology on the left side. On the right side are the *C. compactum* individual growth series (grey curves) and $SGI_{indirect}$ master-chronology (black curve).

Figure 6: Average of (A) Mg/Ca and (B) Ba/Ca variations of the three studied specimens (bold lines). Light colored lines represent the nine transects performed on each specimen. On the upper left side of each part, a 5-year portion of a randomly selected transect presenting the visually determined growth line positions (red vertical lines).

Figure 7: Spearman's correlation coefficients between pairs of transects for each specimen and Element/Ca ratios. Crossed out values correspond to non-significant relationships ($p>0.05$).

Figure 8: Spatial correlations (3-month averages) between *C. compactum* SGI_{direct} and mean seasonal ocean temperatures between 0-100m. Only significant ($p<0.05$) correlation coefficients are represented.

Figures

Figure 1:

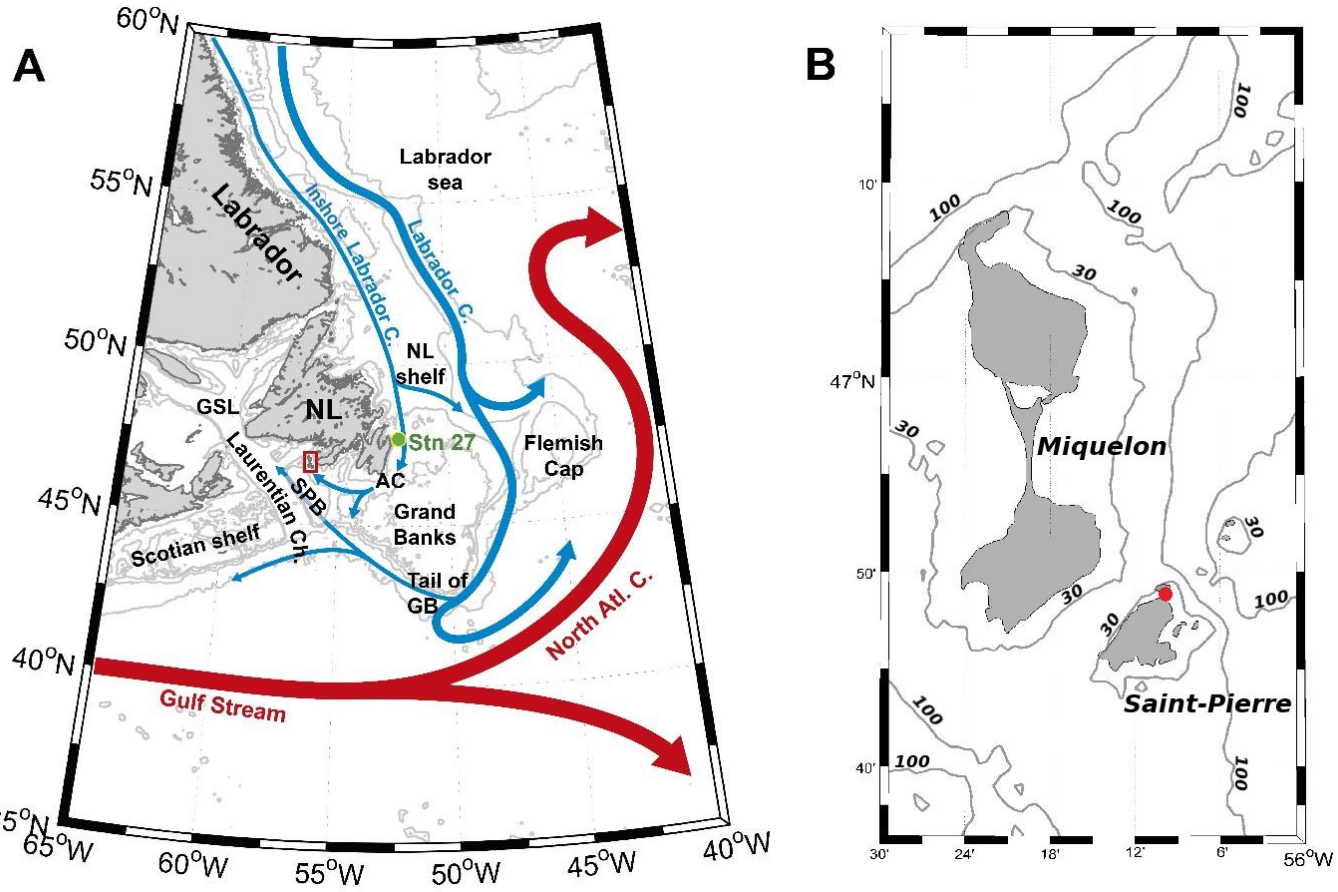

Figure 2:

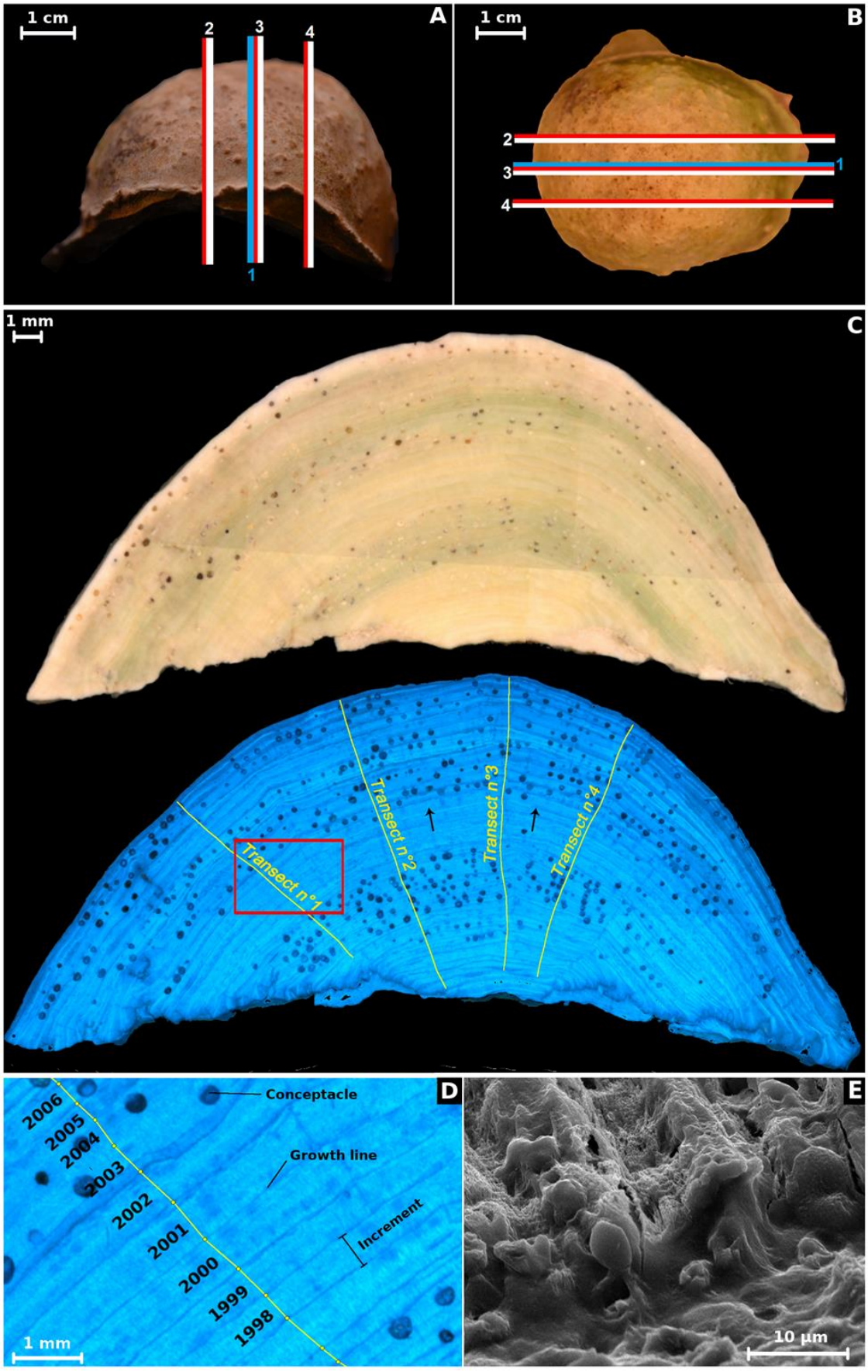
1 cm
A
2
3
4
1
1 cm
B
2
3
4
1
1 mm
C
Transect n°1
Transect n°2
Transect n°3
Transect n°4
Conceptacle
D
2006
2005
2004
2003
2002
2001
2000
1999
1998
Growth line
Increment
1 mm
E
10 µm

Figure 3:

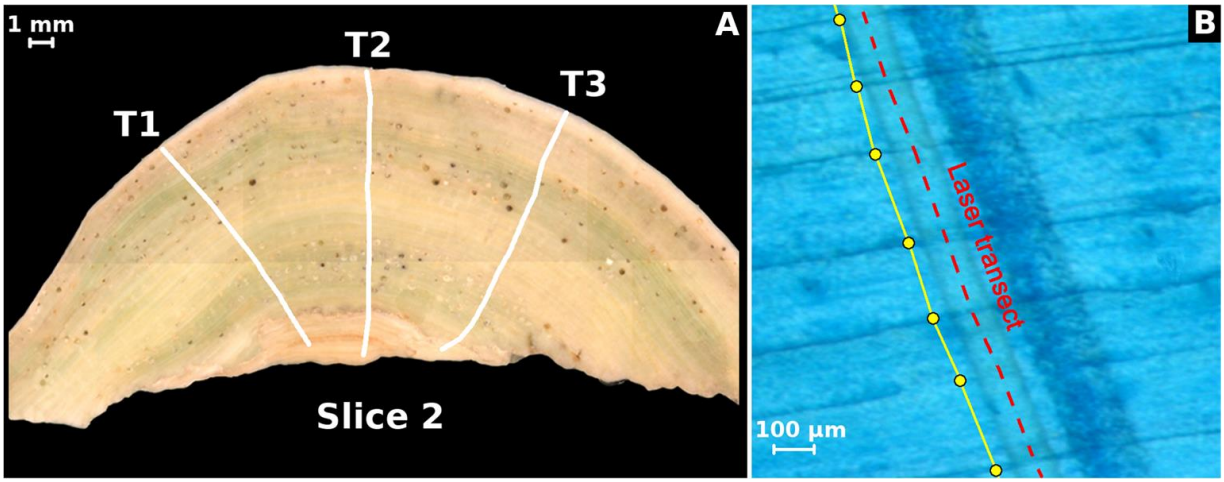

Figure 4:

CC2

T1	T2	T3	T4	T5	
1	0.49	0.34	~~0.01~~	0.48	**T1**
	1	0.46	~~0.28~~	0.48	**T2**
		1	0.5	0.29	**T3**
			1	~~0.25~~	**T4**
				1	**T5**

CC3

T1	T2	T3	
1	0.71	0.58	**T1**
	1	0.8	**T2**
		1	**T3**

CC7

T1	T2	T3	T4	
1	0.75	0.65	~~0.31~~	**T1**
	1	0.56	~~0.23~~	**T2**
		1	~~0.24~~	**T3**
			1	**T4**

CC11

T1	T2	
1	0.55	**T1**
	1	**T2**

CC13

T1	T2	T3	T4	T5	T6	T7	
1	0.56	0.44	0.37	0.43	~~0.11~~	~~0.18~~	**T1**
	1	0.43	~~0.18~~	~~0.26~~	~~0.02~~	0.42	**T2**
		1	0.23	0.25	~~0.29~~	0.50	**T3**
			1	0.55	~~0.12~~	~~0.10~~	**T4**
				1	~~0.21~~	~~0.24~~	**T5**
					1	~~0.38~~	**T6**
						1	**T7**

CC29

T1	T2	T3	T4	
1	~~0.27~~	~~0.35~~	~~0.30~~	**T1**
	1	0.63	0.56	**T2**
		1	0.75	**T3**
			1	**T4**

CC34

T1	T2	T3	T4	T5	T6	
1	0.85	0.70	0.67	0.63	0.62	**T1**
	1	0.68	0.59	0.58	0.61	**T2**
		1	0.72	0.60	0.67	**T3**
			1	0.49	0.51	**T4**
				1	0.64	**T5**
					1	**T6**

Figure 5:

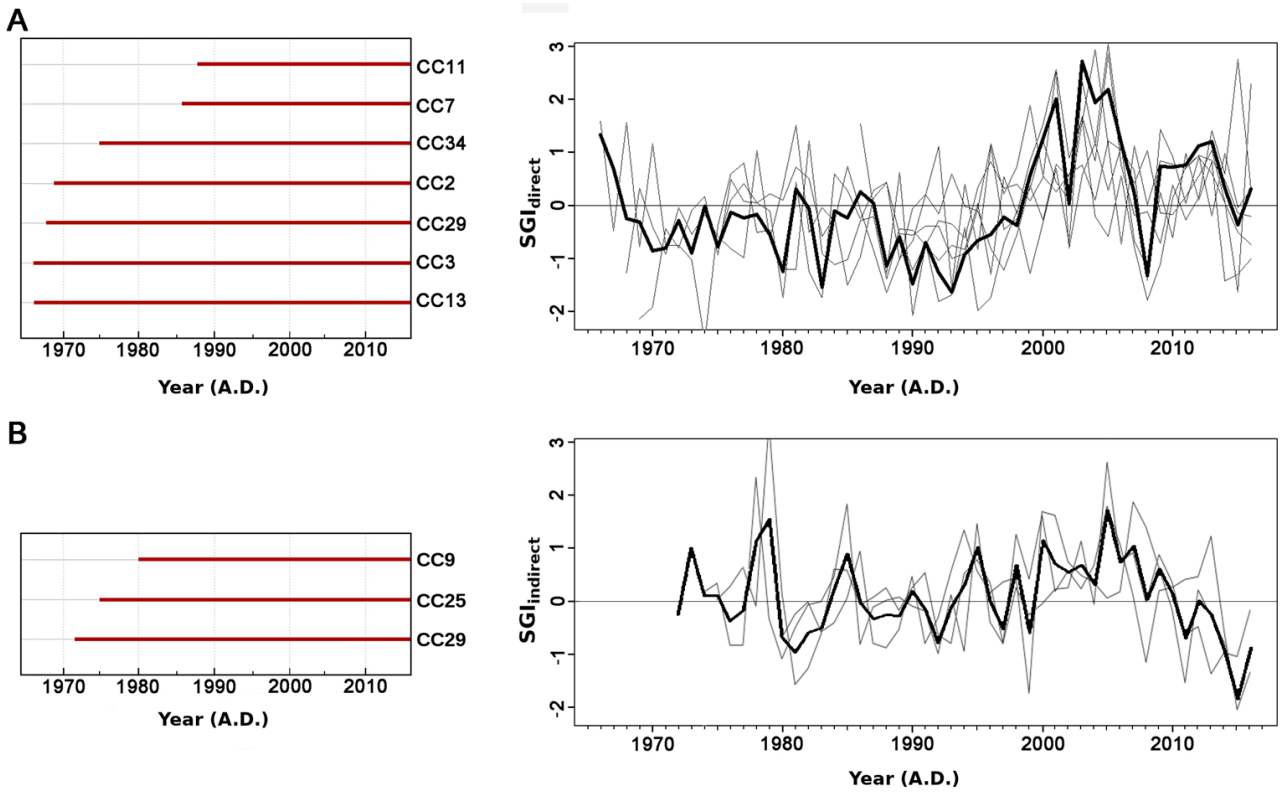
A
CC11
CC7
CC34
CC2
CC29
CC3
CC13
1970
1980
1990
2000
2010
Year (A.D.)
SGI direct
3
2
1
0
-1
-2
1970
1980
1990
2000
2010
Year (A.D.)
B
CC9
CC25
CC29
1970
1980
1990
2000
2010
Year (A.D.)
SGI indirect
3
2
1
0
-1
-2
1970
1980
1990
2000
2010
Year (A.D.)

Figure 6:

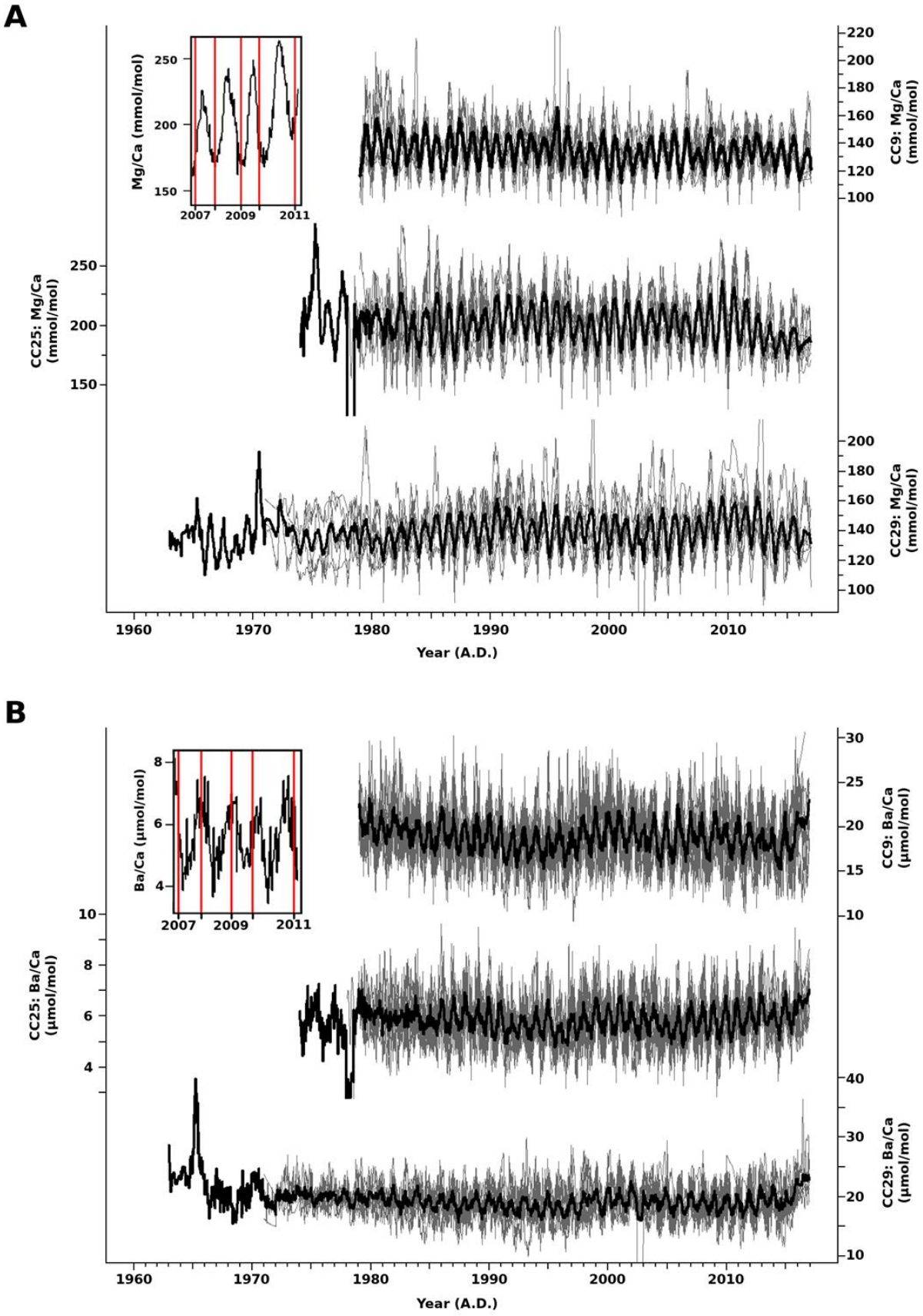
A
Mg/Ca (mmol/mol)
2007
2009
2011
CC25: Mg/Ca (mmol/mol)
CC9: Mg/Ca (mmol/mol)
CC29: Mg/Ca (mmol/mol)
Year (A.D.)
B
Ba/Ca (µmol/mol)
CC25: Ba/Ca (µmol/mol)
CC9: Ba/Ca (µmol/mol)
CC29: Ba/Ca (µmol/mol)
Year (A.D.)

Figure 7:

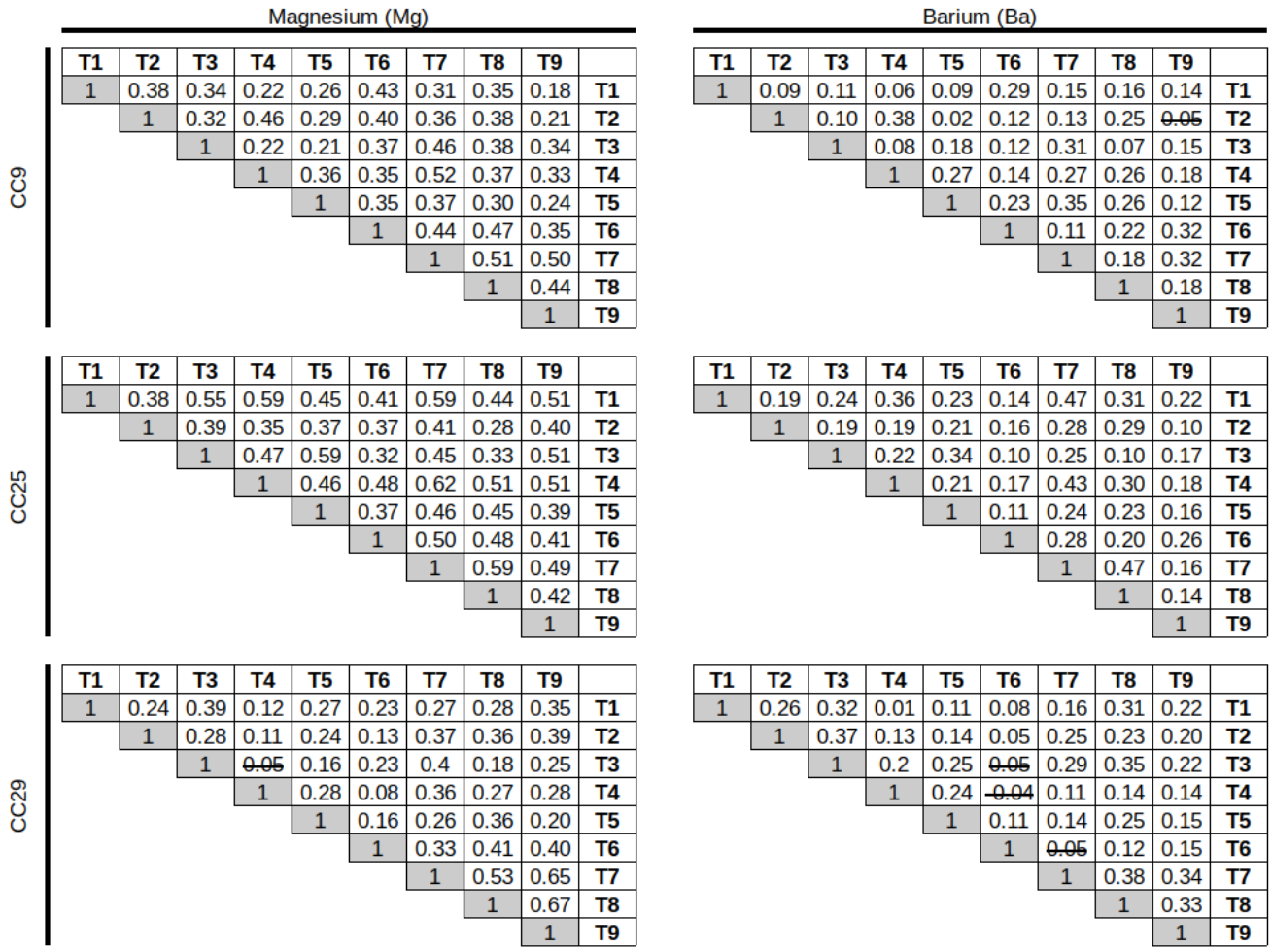

Magnesium (Mg)

CC9

T1	T2	T3	T4	T5	T6	T7	T8	T9	
1	0.38	0.34	0.22	0.26	0.43	0.31	0.35	0.18	**T1**
	1	0.32	0.46	0.29	0.40	0.36	0.38	0.21	**T2**
		1	0.22	0.21	0.37	0.46	0.38	0.34	**T3**
			1	0.36	0.35	0.52	0.37	0.33	**T4**
				1	0.35	0.37	0.30	0.24	**T5**
					1	0.44	0.47	0.35	**T6**
						1	0.51	0.50	**T7**
							1	0.44	**T8**
								1	**T9**

CC25

T1	T2	T3	T4	T5	T6	T7	T8	T9	
1	0.38	0.55	0.59	0.45	0.41	0.59	0.44	0.51	**T1**
	1	0.39	0.35	0.37	0.37	0.41	0.28	0.40	**T2**
		1	0.47	0.59	0.32	0.45	0.33	0.51	**T3**
			1	0.46	0.48	0.62	0.51	0.51	**T4**
				1	0.37	0.46	0.45	0.39	**T5**
					1	0.50	0.48	0.41	**T6**
						1	0.59	0.49	**T7**
							1	0.42	**T8**
								1	**T9**

CC29

T1	T2	T3	T4	T5	T6	T7	T8	T9	
1	0.24	0.39	0.12	0.27	0.23	0.27	0.28	0.35	**T1**
	1	0.28	0.11	0.24	0.13	0.37	0.36	0.39	**T2**
		1	~~0.05~~	0.16	0.23	0.4	0.18	0.25	**T3**
			1	0.28	0.08	0.36	0.27	0.28	**T4**
				1	0.16	0.26	0.36	0.20	**T5**
					1	0.33	0.41	0.40	**T6**
						1	0.53	0.65	**T7**
							1	0.67	**T8**
								1	**T9**

Barium (Ba)

T1	T2	T3	T4	T5	T6	T7	T8	T9	
1	0.09	0.11	0.06	0.09	0.29	0.15	0.16	0.14	**T1**
	1	0.10	0.38	0.02	0.12	0.13	0.25	~~0.05~~	**T2**
		1	0.08	0.18	0.12	0.31	0.07	0.15	**T3**
			1	0.27	0.14	0.27	0.26	0.18	**T4**
				1	0.23	0.35	0.26	0.12	**T5**
					1	0.11	0.22	0.32	**T6**
						1	0.18	0.32	**T7**
							1	0.18	**T8**
								1	**T9**

T1	T2	T3	T4	T5	T6	T7	T8	T9	
1	0.19	0.24	0.36	0.23	0.14	0.47	0.31	0.22	**T1**
	1	0.19	0.19	0.21	0.16	0.28	0.29	0.10	**T2**
		1	0.22	0.34	0.10	0.25	0.10	0.17	**T3**
			1	0.21	0.17	0.43	0.30	0.18	**T4**
				1	0.11	0.24	0.23	0.16	**T5**
					1	0.28	0.20	0.26	**T6**
						1	0.47	0.16	**T7**
							1	0.14	**T8**
								1	**T9**

T1	T2	T3	T4	T5	T6	T7	T8	T9	
1	0.26	0.32	0.01	0.11	0.08	0.16	0.31	0.22	**T1**
	1	0.37	0.13	0.14	0.05	0.25	0.23	0.20	**T2**
		1	0.2	0.25	~~0.05~~	0.29	0.35	0.22	**T3**
			1	0.24	~~-0.04~~	0.11	0.14	0.14	**T4**
				1	0.11	0.14	0.25	0.15	**T5**
					1	~~0.05~~	0.12	0.15	**T6**
						1	0.38	0.34	**T7**
							1	0.33	**T8**
								1	**T9**

Figure 8: